Notas de Física - Volume XI - Nº 1

ABSOLUTE CROSS-SECTIONS FOR SOME (n,p), (n,α) AND (n, 2n) REACTIONS

J. M. F. Jeronymo
Centro Brasileiro de Pesquisas Físicas
Rio de Janeiro, Brazil

G. S. Mani, J. Olkowsky, A. Sadeghi, C. F. Williamson*
Centre d'Etudes Nucléaires, Saclay, France

(Received October, 15, 1963)

Abstract: The reactions $Al^{27}(n,\alpha)Na^{24}$, $Mg^{24}(n,p)Na^{24}$, $Si^{28}(n,p)Al^{28}$, $Co^{59}(n,p)Fe^{59}$, $Co^{59}(n,2n)Co^{58}$, $Co^{59}(n,\alpha)Mn^{56}$, $Ni^{58}(n,p)Co^{58}$ and $Ni^{58}(n,2n)Ni^{57}$ have been studied by an activation method from 12.5 to 21.0 MeV neutron energy. A method of calibrating well type crystals to obtain absolute efficiency is described. The results for absolute cross-sections obtained by this method for the above reactions are compared with statistical model calculations in which the nuclear trasmission coefficients have been derived from an average optical potential extracted from the scattering data.

---

* Present address: Department os Physics, University of Washington, Seattle, Washington.

1. Introduction.

The neutron cross-section is a good test of the statistical theory of nuclear reactions. Unfortunately, due to the crudeness of the model, it would not be possible in individual cases to decide between the statistical model and other types of reaction mechanisms. The best one could attempt to do is to obtain an overall picture of the reaction mechanism by studying a large number of nuclei.

Many cross-section measurements have already been made around 14 MeV neutron energy, the choice of this energy mainly due the availability of intense neutron beams using Crockroft--Walton type accelerators.

Unfortunately the values of cross-section obtained around 14 MeV neutron energies by various laboratories are distressingly inconsistent. The dispersion in the actual values are much larger than the quoted experimental errors. In fig. 1 is shown the results of these measurements for (n,p) reactions; this figure has been drawn on the basis of the recent compilation by Gardner [1]. Fig. 2 shows a similar compilation for (n,α) reactions [2] at 14 MeV. One can see from these two figures the amount of discrepancy that exists among the various measurements. Further very few absolute measurements have been performed as a function of incident neutron energy. Most of the excitation curves found in the literature have been normalised to the 14 MeV data and since the 14 MeV data are themselves so inconsistent, it is at

present not possible to make any detailed analysis of the applicability of the statistical model to neutron induced reactions in this energy region.

A programme of systematic study of absolute reaction cross-sections as a function of neutron energy would hence be very useful and has been initiated at Saclay. This paper gives the first results of this programme.

2. Experimental Method.

2.1. Irradiation: The samples to be irradiated were in the form of cylinders of spectroscopically pure elements of dimensions 10.5 mm in diameter and 49.5 mm long. The samples were mounted on specially constructed holder such that the angle between the axis of the sample and the beam direction could be adjusted to better than 2^{o}. The maximum error in the distance of the sample from the target was of the order of 1 mm. This arrangement allowed up to eight samples to be irradiated simultaneously, with adjacent samples subtending 20^{o} at the target. The target was a titanium-tritium disc with a thickness of about 1 mg/cm^{2}.

Deuteron from the Saclay Van de Graaff having energy of 4.2 MeV were focussed and collimated on to the target to a diameter of around 1.5 mm. The beam current used during the greater part of the experimental was of the order of 4 μA and the target was cooled externally by compressed air. The samples were positioned with their front faces 57 mm from the beam spot.

The neutron flux was monitored by a proton recoil spectrometer. This consisted of a plastic scitillator 2.0 cm in diameter and 1.0 cm thickness mounted on an EMI 6097 photo-multiplier, placed at a distance of 50 cm from the target and subtending an angle of 90^{o} to the beam direction. The proton recoil spectrum was recorded on a 256 channel pulse-height analyser and the resulting spectrum was analysed by the method of Schwartz and Owen [3] to obtain the flux. The beam current was also integrated to provide a check on target deterioration. No appreciable deterioration was observed during the course of the experiment.

A schematic drawing of the irradiation geometry is shown in fig. 3. In fig. 4 is shown a typical proton recoil spectrum from the monitor. In table 1 is given the irradiation time for each sample as well as the time before counting the activity was commenced. In all cases except silicon, eight samples were irradiated simultaneously and the neutron monitor counts were recorded automatically every half hour. In the case of silicon, due to the short lived activity of the reaction products, only one sample was irradiated at a time, and runs were rejected in which the beam current varied by more than 5%.

In the case of cobalt two different irradiation times were necessary because it was very difficult to separate the 845 keV gamma ray of the $Co^{59}(n,\alpha)Mn^{56}$ reaction from the 799 keV gamma ray of the $Co^{59}(n,2n)Co^{58}$ reaction. A short irradiation of about two hours produced predominantly the (n,α) reaction. The small

admixture of the (n, 2n) reaction was subtracted out by decay curve analysis. On the other hand a long irradiation followed by an interval of about a day and a half yielded only the products of the $Co^{59}(n, 2n)Co^{58}$ and the $Co^{59}(n,p)Fe^{59}$ reactions.

All the reactions studied together with half-lives, gamma ray energies and branching ratios are indicated in table 2.

2.2. Counting: The samples were counted in a 4.4 cm × 5.1 cm NaI(Tl) crystal having a cylindrical well 1.3 cm in diameter and 4.01 cm deep. The irradiated samples were placed in a plexiglass holder before counting in order to accurately position the sample inside the well. This holder also served to absorb a part of the unwanted beta activity that accompanies the gamma rays. The external diameter of the cylindrical holder was slightly less than the well diameter and it was bored along its axis to the exact diameter of the samples, leaving an end thickness of 2 mm. The geometry is shown schematically in the inset of fig. 3.

In order to calculate the absolute cross-sections, one must know the efficiency of the gamma spectrometer. The problem of calculating theoretically the efficiency of a well type crystal is formidable even for the case of a point source. For an extended source, taking into account also the source absorption, the mathematical problem becomes impossible. In the present case a further complication is introduced due to the variation of the intensity of the source along its length because of solid

angle effects as well as beam attenuation in the sample during irradiation.

It was decided, because of the above mentioned difficulties, to obtain an empirical measure of the effective efficiency of the crystal for the irradiated sources. A description of the method as well as the results obtained are given in the appendix.

The pulses from the photomultiplier were amplified by conventional electronics and were recorded by a 256-channel analyser. The entire spectrometer was surrounded by 5 cm of lead to reduce the background. The background with an unirradiated sample was measured at frequent intervals. It was found in most cases to be less than a few percent of the counts under the photopeak. The samples were measured in rotation to eliminate any experimental errors and the decay was followed in most cases to a few half-lives.

The gamma spectra were analysed on the IBM 7090 at Saclay as follows. The photopeaks were assumed to have a Gaussian shape while the Compton tails with the backgrounds were assumed to be given by a series of exponentials. The parameters for minimum number of exponentials needed were obtained by a least-squares fit and by comparing the χ^2. The area under the photopeak was then evaluated by the machine and the standard errors were obtained by inverting the normal matrix.

The procedure for obtaining the absolute cross-section is given in the appendix. As can be seen from eq. (A.5), one needs

also to know the angular distribution of the neutrons obtained from the $d(T,n)He^4$ reaction. This was evaluated from the curves given by Jarmie and Seagrave [4]. The final cross-section is quoted with errors obtained from (i) the estimation of the area of the photopeak (ii) the errors in the absolute efficiency determination of the crystal (iii) the errors in the $d(T,n)He^4$ angular distribution (iv) errors in the determination of absolute neutron flux. The maximum error in the energy of the neutrons is of the order of 150 keV.

3. Results.

3.1. Aluminium irradiation: Fig. 5 shows the cross-section for the $Al^{27}(n,\alpha)Na^{24}$ reaction as obtained by us as well as by other laboratories. It can be seen from the figure that there is reasonable agreement in absolute cross-section measurement amongst the various groups.

The solid line in the figure is the statistical model calculations of Mani and Melkanoff [5]. In these calculations the nuclear penetrabilities were obtained from an average optical model potential extracted from the scattering data. For the level density, the Cameron semi-empirical formula [6] was used. Pairing energy corrections were taken into account, the values for the pairing energy being obtained from Cameron [6]. Thus there are no adjustable parameters in the calculation. Since detailed results using this programme will be published soon, we shall not give here the various parameters used. As can be

seen from fig. 5, the theory fits the data energy well.

Since there is reasonable agreement in the values of the $Al^{27}(n,\alpha)Na^{24}$ reaction amongst the various laboratories, we feel that this reaction could be used as a standard against which other reactions could be measured.

3.2. Magnesium irradiation: In the case of magnesium, since we measured the total Na^{24} activity, our cross-section is the sum of the $Mg^{24}(n,p)Na^{24}$, $Mg^{25}(n,d)Na^{24}$ and $Mg^{26}(n,t)Na^{24}$ reactions weighted by the abundance of the respective magnesium isotope. In fig. 6 are shown our results for this measurement together with data from other laboratories. The agreement with other workers is reasonably good.

The full line marked I in the figure is Mani and Melkanoff's calculation for $Mg^{24}(n,p)Na^{24}$ reaction. Curve II is their result for $Mg^{25}(n,d)Na^{24}$ reaction. The cross-section for $Mg^{26}(n,t)Na^{24}$ was less than 10 mb in this energy region. The dotted curve III in the figure is the mean of curves I and II weighted with the respective isotopic abundance. Since the programme cannot in its present from yield the cross-section for two particle emission, they could not estimate the cross-sections for the $Mg^{25}(n,pn)Na^{24}$ and the $Mg^{25}(n,pn)Na^{24}$ reactions. The discrepancy at the higher energies may be due to the neglect of the last two reactions.

3.3. Silicon irradiation: Fig. 7 shows our results for the $Si^{28}(n,p)Al^{28}$ reaction together with data from other sources. A

part of the cross-section for this reaction would be due to the $Si^{29}(n,d)Al^{28}$ and $Si^{30}(n,t)Al^{28}$ reactions but since the natural abundance of Si^{29} and Si^{30} are 4.7% and 3.1%, respectively, we assume that within our errors, the data quoted is mainly from the $Si^{28}(n,p)Al^{28}$ reaction. The calculations of Mani and Melkanoff also support this view. The full curve shown in fig. 7 is their calculation for the $Si^{28}(n,p)Al^{28}$ reaction and it agrees fairly well with the experiment.

3.4. Cobalt irradiation: Our results for $Co^{59}(n,p)Fe^{59}$ reaction are shown in fig. 8. The full line curve in fig. 8 is the calculation of Mani and Melkanoff. The agreement is not very good. In fig. 9 are shown the results of $Co^{59}(n,\alpha)Mn^{56}$ reaction while the full curve in the figure is the statistical model calculation described above. The theory yields a cross-section about four times less than the experimental value. Since the maximum experimental cross-section is only of the order of 20 mb, this discrepancy should not perhaps be taken too seriously. It must be remarked here that the theory does reproduce the large difference in the cross-section between the $Co^{59}(n,p)Fe^{59}$ reaction (of the order 100 to 600 mb) and the $Co^{59}(n,\alpha)Mn^{56}$ reaction (of the order of 8 to 25 mb).

In fig. 10 we show our results for the $Co^{59}(n,2n)Co^{58}$ reaction. The radioactive nucleus Co^{58} has an isomeric state at 25 keV excitation energy having a half-life [7] of 9.2 hours. This level decays entirely by integral transition to the

ground state which has a half-life of 71 d. Since the samples were counted a day and a half after irradiation, the results obtained by us are for the total (n,2n) cross-section.

3.5. Nickel irradiation: The results for $Ni^{58}(n,p)Co^{58}$ reaction are shown in fig. 11. As mentioned above, the cross-sections are for the total (n,p) reaction going to both the isomeric and the ground state. The full line in fig. 11 is the theoretical estimate by Mani and Melkanoff. The agreement is not very good. Further our cross-sections seem to be much smaller than previously quoted values. We have not been able to find the reason for this discrepancy.

We find a factor of five between the theoretical prediction and our experiment. We think that this is due to shell effects, since we find the same behaviour with cobalt also. A similar discrepancy has been noted by Allan [8] around the Z = 28 region of nucleides. Since the optical model potential does not exhibit any strong behaviour in the closed shell regions, we feel that this discrepancy may be mainly due to the inadequacy of the level density formula for these nuclei. It would be very interesting to determine the cross-section for these nuclei for much lower energies as well as to find if similar effects exist for other closed shell nuclei.

The results for the $Ni^{58}(n,np)Co^{57} + Ni^{58}(n,d)Co^{57} + Ni^{58}(n,pn)Co^{57}$ reactions are shown in fig. 12. In fig.13 we show the results of $Ni^{58}(n,2n)Ni^{57}$ reaction. The calculations

of Mani and Melkanoff as mentioned earlier, cannot evaluate each separate two particle emission cross-section but could yield only the cross-sections for the sums of the reactions $Ni^{58}(n, np)Co^{57}$ + + $Ni^{58}(n,2n)Ni^{57}$ and $Ni^{58}(n,pn)Co^{57}$ + $Ni^{58}(n,pp)Fe^{57}$. In fig. 12, the solid line I is their calculation for $Ni^{58}(n,pn)Co^{57}$ + + $Ni^{58}(n,pp)Fe^{57}$. We have assumed that two proton emission is less probable than neutron emission and hence this curve yields the cross-section for the (n,pn) reaction only. The curve marked II in fig. 13 is their results for the $Ni^{58}(n,d)Co^{57}$ reaction. The dotted curved III was obtained as follows. We subtracted the experimental (n,2n) cross-section from their theoretical evaluation of the (n,2n) + (n,np) cross-section and the result is plotted as curve III for the (n,np) reaction only. Curve IV in fig. 12 is the addition of curves I - III to obtain the total (n,d)+ + (n,pn) + (n,np) cross-section. The agreement with experiment is reasonably good. The full line in fig. 13 is the theoretical estimate for the (n,2n) + (n,np) cross-section.

In table 3 we give the results of all the cross-sections measured in this work together with probable error.

The fact that in light and medium weight nuclei, the statistical model explains reasonably well the trends in the neutron induced reaction cross-sections is indeed encouraging. More work is needed, especially around the closed shell regions and for heavier nuclei before one could evaluate the reaction mechanism involved in neutron induced reactions.

Acknowledgements:

We would like to express our thanks to Mr. B. Olkowsky and his group for their help in running the Van de Graaff.

* * *

APPENDIX

In this appendix we give the equations that were used for evaluating the absolute cross-section. Since the efficiency we measured also included the absorption of the gamma rays in the samples used in the neutron experiment, we define this as the "effective" efficiency.

Let $\varphi_M(t)$ be the flux at the monitor at time t, $\sigma_T(\theta)$ be the number of neutrons per unit solid angle emerging in the direction θ from the target, Ω_M be the solid angle of the monitor with respect to the target which is assumed to be a point source and $\Omega_S(x)$ be the solid angle subtended by the sample at the point x along its axis (see fig. 14). The flux $\varphi_S(x, t)$ at the point x in the sample at time t is given by

$$\varphi_M(t) = \left\{\sigma_t(\theta_M)\, \Omega_M/A_M\right\} K\, I\,(t) \qquad (A.1)$$

$$\varphi_S(x, t) = \left\{\sigma_T(\theta_S)\, \Omega_S(x)/A_S\right\}\ K\, I\,(t)\, e^{-\lambda_S x} \qquad (A.2)$$

where A_M and A_S are the cross-sectional areas of the monitor and the sample, respectively, λ_S the mean free path of neutrons in

the sample, I(t) the beam current at time t, and K is the constant of proportionality. The quantities θ_M and θ_S refer to the angles the axis of the monitor and the sample have with the beam direction, respectively. Here we assume that t = 0 at the commencement of irradiation. From (A.1) and (A.2) we get

$$\varphi_S(x,t) = \frac{\sigma_T(\theta_S)}{\sigma_T(\theta_M)} \frac{\Omega_S(x)}{\Omega_M} \frac{A_M}{A_S} \varphi_M(t) e^{-\lambda_S x} \qquad (A.3)$$

Let T_γ be the total irradiation time, λ_g be the decay constant of the radioactive nuclei produced in the reaction and N_S be the total number of nuclei in the sample. Then we get for the total activity at the end of irradiation time T_γ from the strip between x and x + d x in the sample

$$A(s,T_\gamma) = \sigma_R N_S \frac{A_M}{A_S} \frac{\sigma_T(\theta_S)}{\sigma_T(\theta_M)} \frac{\Omega_S(x)}{\Omega_M} e^{-\lambda_S x} e^{-\lambda_g T_\gamma} \int_0^{T_\gamma} \varphi_M(t) e^{\lambda_g t} dt \qquad (A.4)$$

Here σ_R is the cross-section for the reactions induced by the neutrons. We assume here that the neutrons have unique energy and that the sample is composed of only one type of nuclei. The extention to more general case is straightforward. If the counting of the sample begins at $t = T_\gamma + T_W$ and ends at $t = T_\gamma + T_W + T_C$, then the total number of counts one obtains under the photopeak of the gamma energy E_γ is given by

$$C = B_g(E_\gamma) \lambda_g \int_0^{\ell} dx \int_{T_W}^{T_C+T_W} A(x,T_\gamma) \varepsilon(x,E_\gamma) e^{-\lambda_g t} dt$$

$$= B_g \sigma_R N_S \frac{A_M}{A_S} \frac{\sigma_T(\theta_S)}{\sigma_T(\theta_M)} e^{-\lambda_g T_\gamma} e^{-\lambda_g T_W} (1 - e^{-\lambda_g T_c})/\Omega_M$$

$$\times \left\{ \int_0^T \varphi_M(t) e^{+\lambda_g t} \, dt \right\} \int_0^\ell dx \, \Omega_S(x) \, e^{-\lambda_S x} \, \varepsilon(x, E_\gamma) \, . \qquad (A.5)$$

Here $B_g(E_\gamma)$ denotes the fraction of the activity yielding the gamma ray of energy E_γ and can be obtained from the decay scheme. The quantity $\varepsilon(x, E_\gamma)$ is the absolute "effective" efficiency of the well crystal for a disc source of diameter equal to the sample diameter emitting gamma rays of energy E_γ, kept at a distance x from the bottom of the well.

Due to the factor $e^{-\lambda_S x} \Omega_S(x)$ that occurs in (A.5), the sample does not have a uniform activity. Since $\varepsilon(x, E_\gamma)$ is a function of the distance from the bottom of the well, the way in which the sample is placed in the crystal becomes important. In our experiment the face of the sample nearest to the target was placed at the bottom of the well. The above definition of x corresponds to this situation.

From (A.5) it is seen that one can obtain the absolute cross-section, provided one knows how to evaluate λ_S, $\varepsilon(x, E_\gamma)$ as well as the integral

$$F(T_\gamma) = \int_0^{T_\gamma} \varphi_M(t) e^{+\lambda_g t} \, dt \qquad (A.6)$$

We give below the method we used for evaluating these three quantities.

The mean free path of neutrons in the sample depends upon

the total cross-section for neutrons in the sample. If σ_T be the total cross-section, then assuming good geometry

$$\lambda_S = N_S' \sigma_T \qquad (A.7)$$

where N_S' is the number of atoms per cubic centimeter in the sample. Since the nonelastic cross-section σ_{nel} is greater than the elastic cross-section, σ_{el}, we have assumed that $\sigma_T \approx \sigma_{nel}$ and for σ_{nel} we use the approximate formula

$$\sigma_{nel} \simeq \pi(R + \lambda\!\!\!^{-})^2 \ . \qquad (A.8)$$

The approximation (A.8) is justified since the beam attenuation is very small, of the order of a few percent.

The quantity $F(T_\gamma)$ defined in (A.6) was evaluated as follows. For all cases except silicon irradiation, the monitor counts was recorded every half-hour and over this period the flux was assumed constant. If T_M denotes this period and n denotes the n^{th} such measurement yielding the number of monitor counts C_n, then

$$F(T_\gamma) = \frac{(1 - e^{-\lambda_g T_m})}{T_M \lambda_g} \sum_{n=1}^{T_\gamma/T_M} C_n e^{+n\lambda_g T_m} \qquad (A.9)$$

Finally the efficiency factor $\epsilon(x, E_\gamma)$ was derived as follows. Several source holders were made from aluminium having exactly the same diameter as the sample. Various radioactive sources were made by placing a drop of the appropriate solution containing the source in the centreof the source holder. After the solution had completely dried, the holders were sealed with

their lids in position. The calibration was performed by counting the sample in standard geometry with a 10.2 cm × 10.2 cm NaI(Tℓ) crystal. This calibration was accurate to about ± 15%.

An unirradiated sample of each element studied was cut into nine pieces, each 5 mm long and one piece 2 mm long. The position of the standard source could then be varied in steps of 5 mm along the depth of the well under conditions similar to those in the experiment. The experimental arrangement is shown in fig. 14. The efficiency $\varepsilon(x, E_\gamma)$ could then be obtained by measuring the area under the photopeak.

Figs. 15 and 16 show curves of $\varepsilon(x, E_\gamma)$ for cobalt and aliminium absorbing samples as a function of x, the depth in cm from the bottom of the well for various values of gamma ray energies, E_γ. Figs. 17 and 18 show values of $\varepsilon(x, E_\gamma)$ for cobalt and aluminium samples as a function of E_γ for various values of x. The peculiar shape of the low energy curves in figs. 15 and 16 is due to sample absorption of gamma rays, end effects as well as light absorption in the crystal.

Finally the integral

$$\int_0^{\ell} dx\, e^{-\lambda_S x}\, \varepsilon(x)\, \Omega_S(x)$$

was evaluated numerically.

TABLE I

Details regarding the irradiation

Sample	Irradiation time	Waiting time	Counting time	Reaction
Aluminium	9.75 hrs	$\geqslant$ 27 min	5 min	$Al^{27}(n,\alpha)Na^{24}$
Magnesium	12.3 hrs	$\geqslant$ 45 min	5 min	$Mg^{24}(n,p)Na^{24}$ + $Mg^{24}(n,d)Na^{24}$ + $Mg^{26}(n,t)Na^{24}$
Silicon	5 min	1 min	5 min	$Si^{28}(n,p)Al^{28}$
Cobalt	2.0 hrs	$\geqslant$ 40 min	5 min	$Co^{59}(n,\alpha)Mn^{56}$
Cobalt	12.25 hrs	$\geqslant$ 48 hrs	variable	$Co^{59}(n,2n)Co^{58}$ and $Co^{59}(n,p)Fe^{59}$
Nickel	11.5 hrs	> 30 min	variable	$Ni^{58}(n,p)Co^{58}$ and $Ni^{58}(n,2n)Ni^{57}$

TABLE II

Details regarding the reactions studied

Reaction	Half life	Gamma energy (keV)	Q-value (MeV)	Remarks
$Al^{27}(n,\alpha)Na^{24}$	15 hours	1368, 2754	- 3.138	We used only the 1368 keV gamma ray.
$Mg^{24}(n,p)Na^{24}$	15 hours	1368, 2754	- 4.783	We used only the 1368 keV gamma ray
$Mg^{25}(n,d)Na^{24}$			- 9.838	
$Mg^{26}(n,t)Na^{24}$			-14.693	
$Si^{28}(n,p)Al^{28}$	2.3 min	1780	- 3.866	
$Co^{59}(n,\alpha)Mn^{56}$	2.576 hrs	845,1810,2130	+ 0.305	We used only the 845 keV gamma ray
$Co^{59}(n,2n)Co^{58}$	71 days	799,1664,863	-10.502	We used the 800 keV gamma ray. We observed only the ground state and not the isomeric state.
$Co^{59}(n,p)Fe^{59}$	45 days	191,1098,1289	- 0.780	We used the 1098 keV gamma ray
$Ni^{58}(n,p)Co^{58}$	71 days	799,1664,863	+ 0.365	We used the 800 keV gamma ray. We observed only the ground state and not the isomeric state.
$Ni^{58}(n,2n)Ni^{57}$	36 hours	128,1380,1910	-11.935	

TABLE III

Absolute cross-section for neutron induced reactions studied in this work

Neutron Energy MeV	CROSS-SECTION (mb)							
	$Al^{27}(n,\alpha)Na^{24}$	$Mg^{24}(n,p)Na^{24}$ + $Mg^{25}(n,d)Na^{24}$ + $Mg^{26}(n,t)Na^{24}$	$Si^{28}(n,p)Al^{28}$	$Co^{59}(n,\alpha)Mn^{56}$	$Co^{59}(n,p)Fe^{59}$	$Co^{59}(n,2n)Co^{58}$	$Ni^{58}(n,p)Co^{58}$	$Ni^{58}(n,2n)Ni^{57}$
12.55±0.2	115 ± 12	255 ± 30	197 ± 25	25 ± 3			130 ± 15	38 ± 4
13.55±0.2	115 ± 12	283 ± 35	189 ± 25	26 ± 3	639 ± 75	232 ± 30	125 ± 15	45 ± 4
14.90±0.2	107±11	195 ± 24	181 ± 20	26 ± 3	534 ± 70	508 ± 70	122 ± 15	39 ± 4
16.50±0.2	84 ± 9	177 ± 22	125 ± 14	20 ± 3	428 ± 60	640 ± 68	175 ± 21	34 ± 4
18.15±0.2	64± 7	158 ± 20	140 ± 16	19 ± 3	195 ± 30	725 ± 85	261 ± 31	24 ± 3
19.60±0.2	52± 7	134 ± 18	75 ± 10	11 ± 2	120 ± 14	734 ± 85	248 ± 30	19 ± 3
20.60±0.2	37±6	140 ± 20	88 ± 10	11 ± 2	105 ± 10	753 ± 90	275 ± 33	8 ± 2
21.00±0.2	31 ± 6	122 ± 14	79 ± 10	8 ± 2	68 ± 10	620 ± 75	273 ± 32	1 ± 1

References:

1. D. G. Gardner, Nuclear Physics 29 (1962) 373.
2. G. S. Mani (unpublished).
3. Schwartz and Owen, Fast neutron Physics, Vol. I, Edited by Marion J. B. and Fowler J. L. (Interscience publishers, 1960).
4. N. Jarmie and J. D. Seagrave, Charged Particle cross-sections, Los Alamos report LA-2014.
5. G. S. Mani and M. A. Melkanoff, Proceedings of International Conference on direct interactions, Padua, 1962.
6. A. G. W. Cameron, Can. J. Phys. 35 (1957) 666.
7. D. Strominger, J. M. Hollander and G. T. Seaborg, Rev. Mod. Phys. 30 (1958) 585.
8. D. L. Allen, Nuclear Physics 24 (1961) 274.
9. S. G. Forbes, Phys. Rev. 88 (1952) 1309.
10. I. Kumabe and R. W. Fink, Nuclear Physics 15 (1960) 316.
11. G. S. Mani, G. J. McCallum and A. T. G. Fergusson, Nuclear Physics 19 (1960) 535.
12. S. Yasumi, J. Phys. Soc. Japan 12 (1957) 443.
13. J. A. Grundl, R. L. Henkel and B. L. Perkins, Phys. Rev. 109 (1958) 425.
14. A. Poularikas and R. W. Fink, Phys. Rev. 115 (1959) 989.
15. A. V. Cohen and P. H. White, Nuclear Physics 1 (1956) 73.
16. B. L. Cohen, Phys. Rev. 81 (1951) 184.
17. E. B. Paul and R. L. Clarke, Can. J. Phys. 31 (1953) 267.
18. J. B. Marion, R. M. Brugger and R. A. Chapman, Phys. Rev. 101 (1956) 294.
19. I. L. Preiss and R. W. Fink, Nuclear Physics 15 (1960) 326.
20. R. J. Howerton, Tabulated Neutron cross-sections, Part. I, Vol. I and Vol. II, U.C.R.L. - 5226 (1958).
21. K. H. Purser and E. W. Titterton, ANU/p-300, Nov. 1958.
22. D. L. Allen, Proc. Phys. Soc. (London) A70 (1957) 195.

* * *

Figure Captions:

Fig. 1. Total cross-section for (n,p) reactions at 14 MeV neutron energy obtained by various laboratories. The full line for each nucleus is the total dispersion in the experimental values found in literature.

Fig. 2. Total cross-section for (n,α) reactions at 14 MeV neutron energy obtained by various laboratories for A < 150. The full line for each nucleus represents the total dispersion in the experimental values found in literature.

Fig. 3. Schematic drawing of the irradiation geometry. The inset shows the plexiglass holder and a typical sample.

Fig. 4. A typical monitor proton recoil spectrum.

Fig. 5. Total cross-section for the reaction $Al^{27}(n,\alpha)Na^{24}$

◊ present work

△ Forbes [9]

♦ Kumabe et al [10]

\+ Mani et al [11]

□ Yasumi [12]

◊ Grundl et al [13]

◊ Poularikas and Fink [14]

The full line is from calculations of Mani and Melkanoff [5].

Fig. 6. Total cross-section for the reaction $Mg^{24}(n,p)Na^{24} + Mg^{25}(n,d)Na^{24} + Mg^{26}(n,t)Na^{24}$.

◊ Present data

◊ Cohen and White [15]

♦ B. L. Cohen [16]

◊ Paul and Clarke [17]

The curves I, II and III are obtained from theoretical calculations of Mani and Melkanoff [5] and are explained in the text.

Fig. 7. Total cross-section for the reaction $Si^{28}(n,p)Al^{28}$.

◊ Present data ◊ Cohen and White [15]

◊ Paul and Clarke [17] ◊ Marion et al [18]

◊ B. L. Cohen [16]

The full line is the calculation of Mani and Melkanoff [5].

Fig. 8. Total cross-section for the $Co^{59}(n,p)Fe^{59}$ reaction.

◊ Present data ◊ Allen [8] ◊ Preiss and Fink [19]

The full curve is the calculation of Mani and Melkanoff.

Fig. 9. Total cross-section for the $Co^{59}(n,\alpha)Mn^{56}$ reaction.

◊ Present data ◊ Howerton [20] ◊ Paul and Clarke [17]

The full curve is the calculation of Mani and Melkanoff.

Fig. 10. Total cross-section for the $Co^{59}(n,2n)Co^{58}$ reaction.

Fig. 11. Total cross-section for the $Ni^{58}(n,p)Co^{58}$ reaction.

◊ Present data ◊ Pulser and Titterton [21]

× Allen [8] ◊ Allen [22]

□ Preiss and Fink [19]

The full line is the calculation of Mani and Melkanoff.

Fig. 12. Total cross-section for $Ni^{58}(n,np) + Ni^{58}(n,d) + Ni^{58}(n,pn)$ reaction.

◊ Present data ◊ Allen [22] × Preiss and Fink [19]

The curves I, II, III and IV are obtained from calculations of Mani and Melkanoff and are explained in the text.

Fig. 13. Total cross-section for $Ni^{58}(n,2n)Ni^{57}$ reaction.

◊ Present data

■ Preiss and Fink [19]

◊ Howerton [20]

◊ Cohen [16]

◊ Paul and Clarke [17]

The full line is the theoretical estimate for the $Ni^{58}(n,2n)Ni^{57}$ + + $Ni^{58}(n,pn)Co^{57}$ reaction by Mani and Melkanoff.

Fig. 14. Schematic drawing of the experimental disposition for determination of efficiency and total cross-section.

Fig. 15. Absolute effective efficiency $\varepsilon(x, E_\gamma)$ for well type crystal as a function of x, the distance from the bottom of the well, for various gamma energies. An aluminium absorber was used.

Fig. 16. Absolute effective efficiency $\varepsilon(x, E_\gamma)$ for well type crystals as a function of x, the distance from the bottom of the well, for various gamma energies. Cobalt absorber was used.

Fig. 17. Absolute effective efficiency $\varepsilon(x, E_\gamma)$ for well type crystals as a function of E_γ, the gamma ray energy, for various values of x with aluminium as absorber.

Fig. 18. Absolute effective efficiency $\varepsilon(x, E_\gamma)$ for well type crystals as a function of E_γ, the gamma ray energy, for various values of x, with cobalt as absorber.

* * *

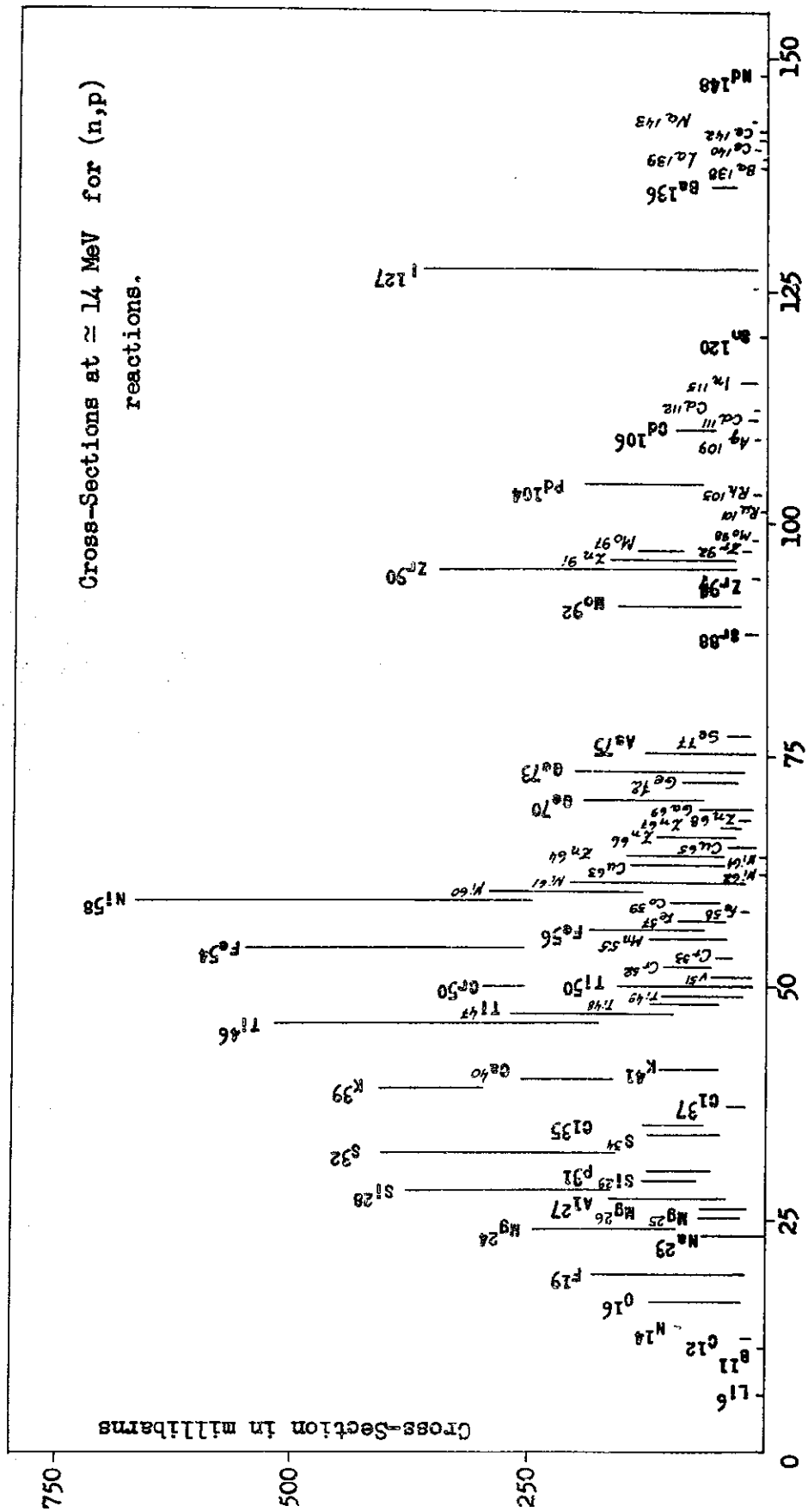
Cross-Sections at ≃ 14 MeV for (n,p)
reactions.
Cross-Section in millibarns
750
500
250
0
25
50
75
100
125
150
MASS NUMBER
Li6
B11
C12
N14
O16
F19
Ne23
Mg24
Mg25
Mg26
Al27
Si28
Si29
P31
S32
S34
Cl35
Cl37
K39
K41
Ca40
Ti46
Ti47
Ti48
Ti49
Ti50
V51
Cr50
Cr52
Mn55
Fe54
Fe56
Fe57
Co59
Ni58
Ni60
Ni61
Ni62
Cu63
Cu65
Zn64
Zn66
Zn67
Zn68
Ga69
Ge72
Ge73
As75
Se77
Br80
Mo92
Zr90
Zr94
Zr96
Mo97
Mo98
Ru100
Rh103
Pd104
Ag109
Cd106
Cd111
Cd112
In115
Sn120
I127
Ba136
Ba138
La139
Ce140
Ce142
Nd143
Nd148

FIG. 1

Experimental data for (n, α) reactions around 14 MeV neutron energy for A < 150.

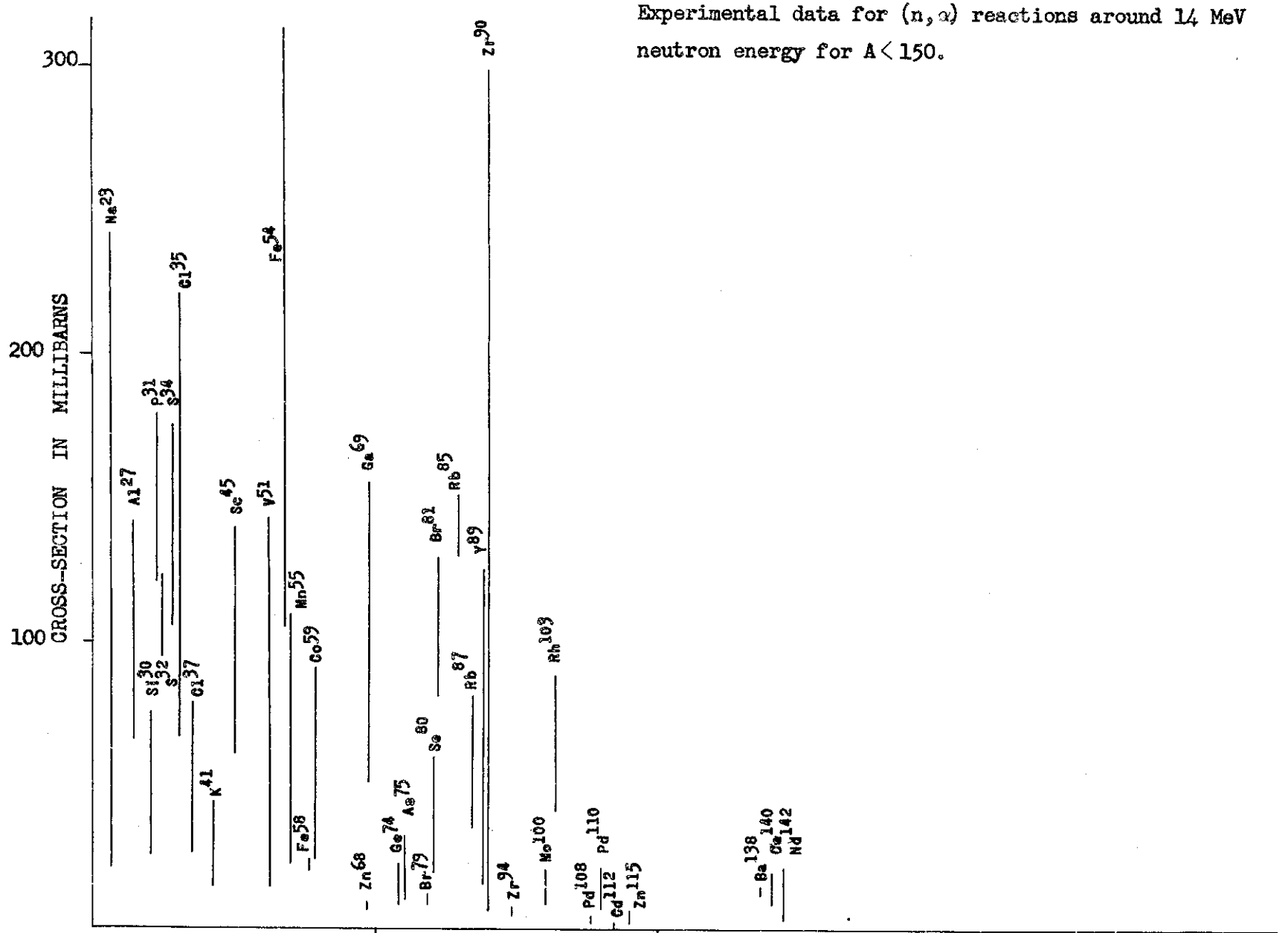

FIG. 2

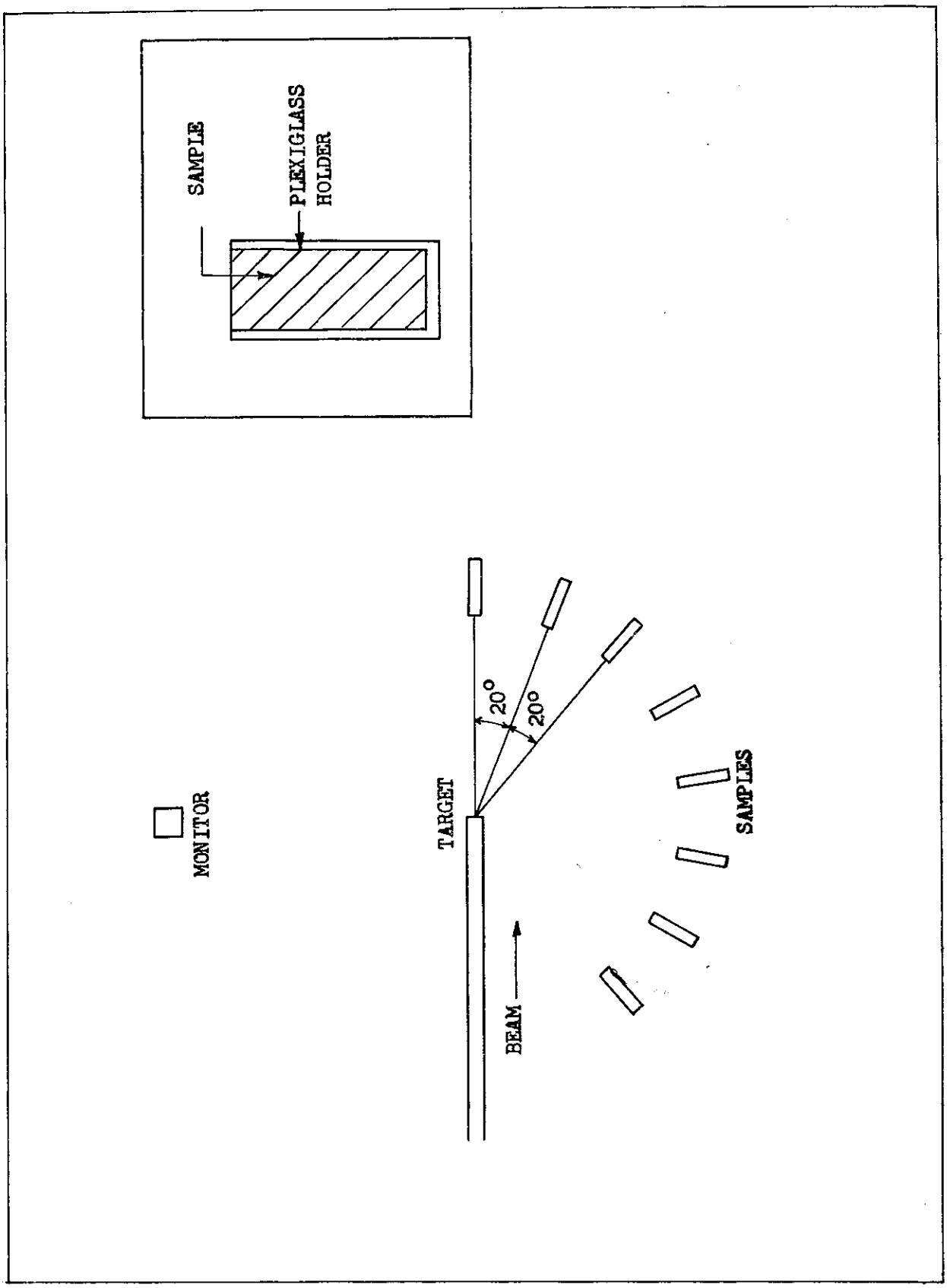
SAMPLE
PLEXIGLASS HOLDER
MONITOR
TARGET
20°
20°
BEAM
SAMPLES

FIG. 3

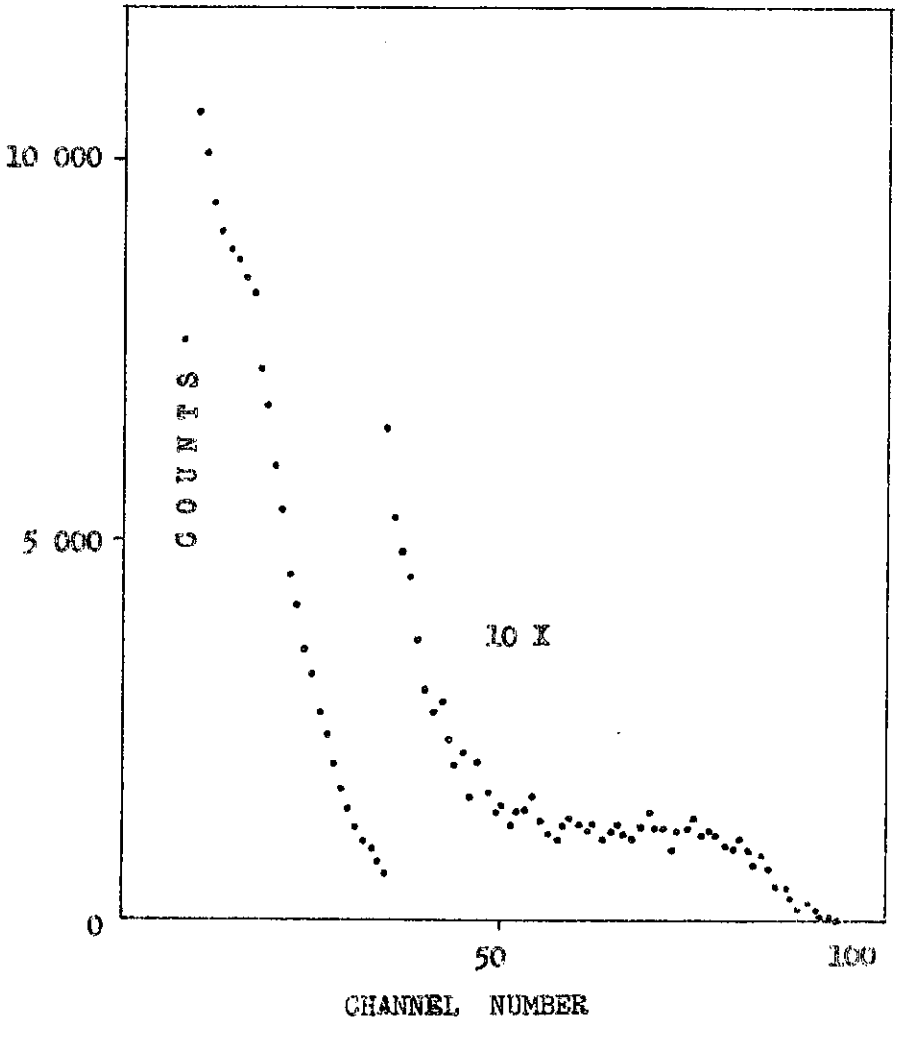

FIG. 4

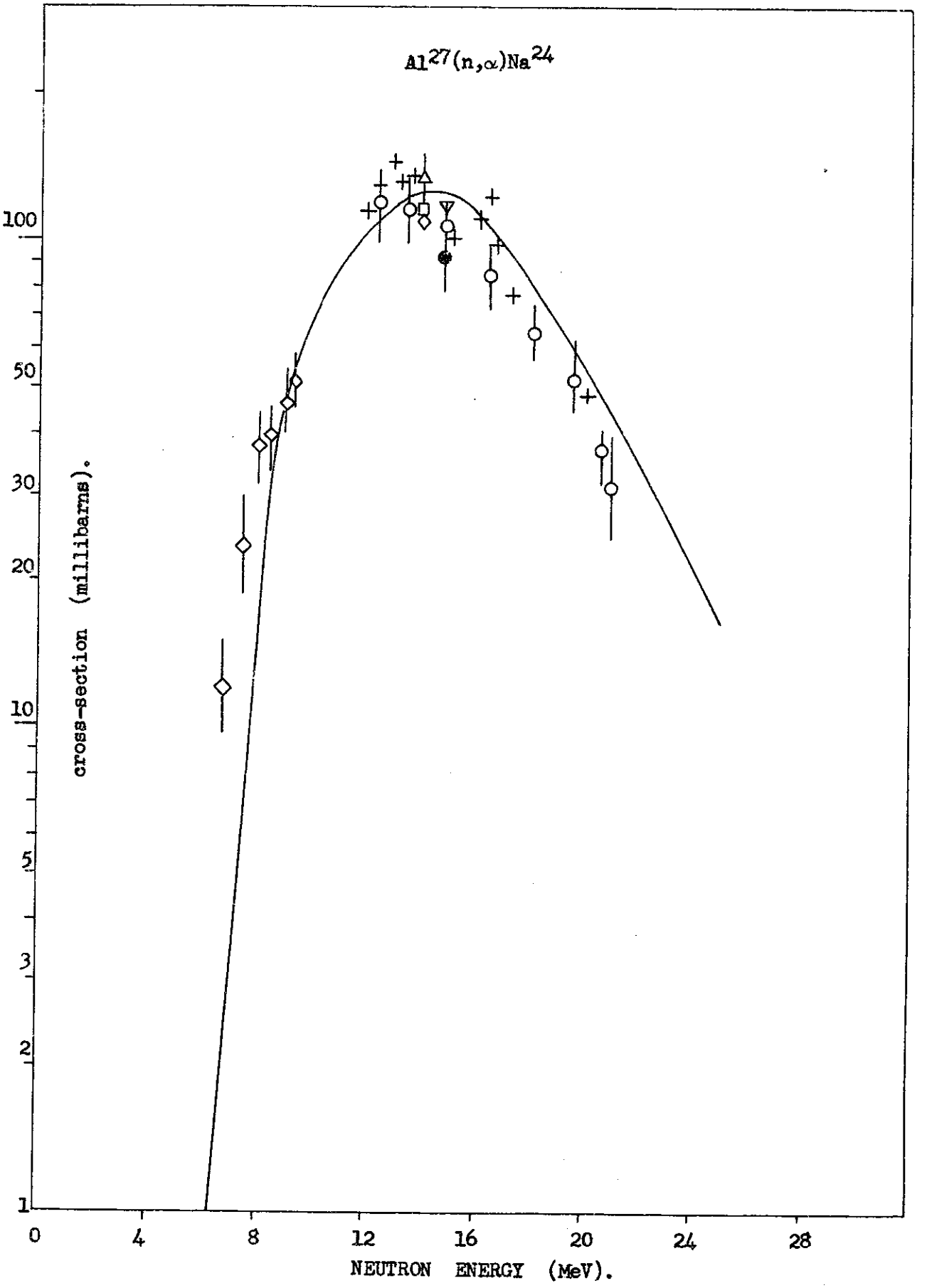
$Al^{27}(n,\alpha)Na^{24}$
cross-section (millibarns).
100
50
30
20
10
5
3
2
1
0
4
8
12
16
20
24
28
NEUTRON ENERGY (MeV).

FIG. 5

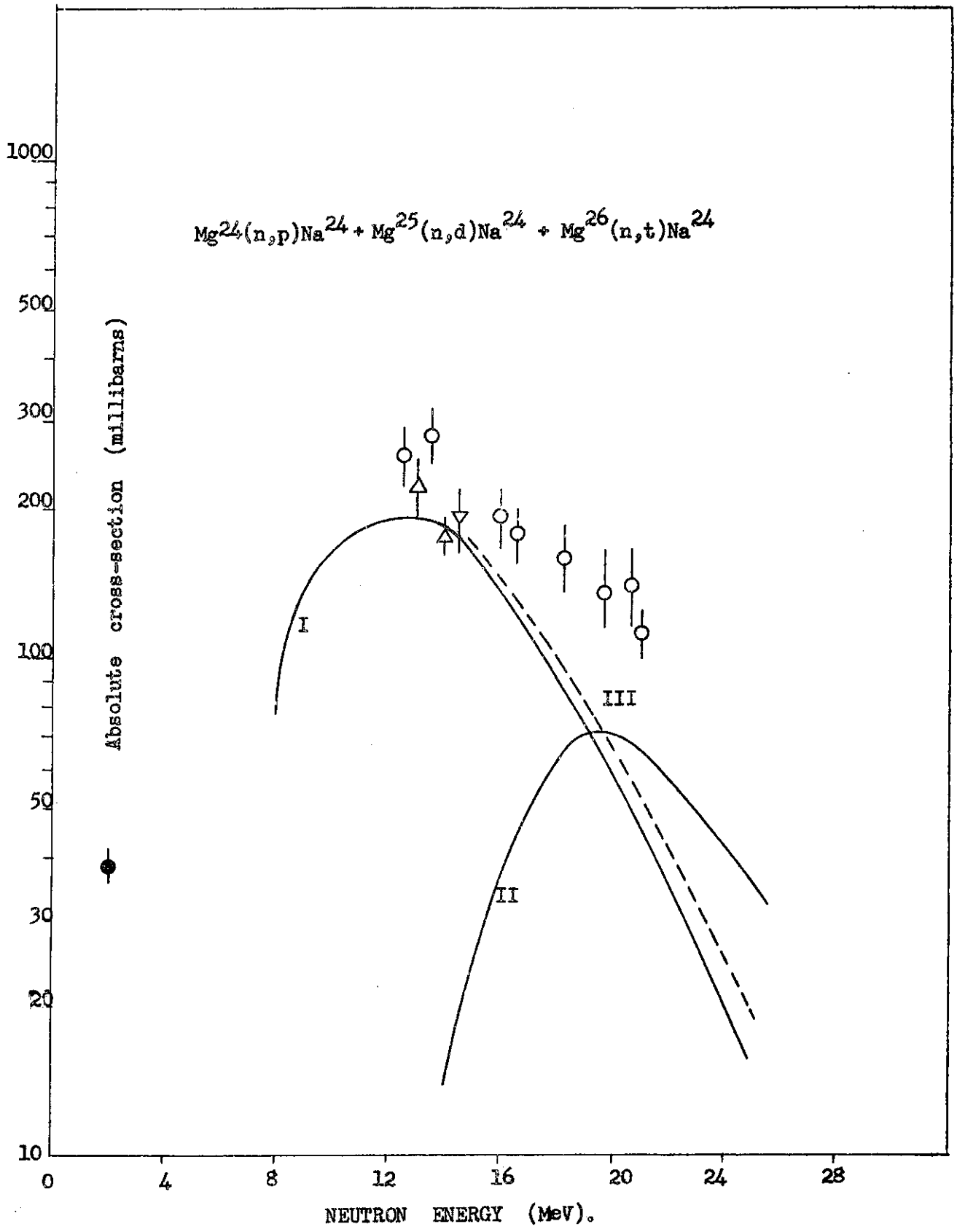
$Mg^{24}(n,p)Na^{24} + Mg^{25}(n,d)Na^{24} + Mg^{26}(n,t)Na^{24}$
Absolute cross-section (millibarms)
1000
500
300
200
100
50
30
20
10
0
4
8
12
16
20
24
28
NEUTRON ENERGY (MeV).
I
II
III

FIG. 6

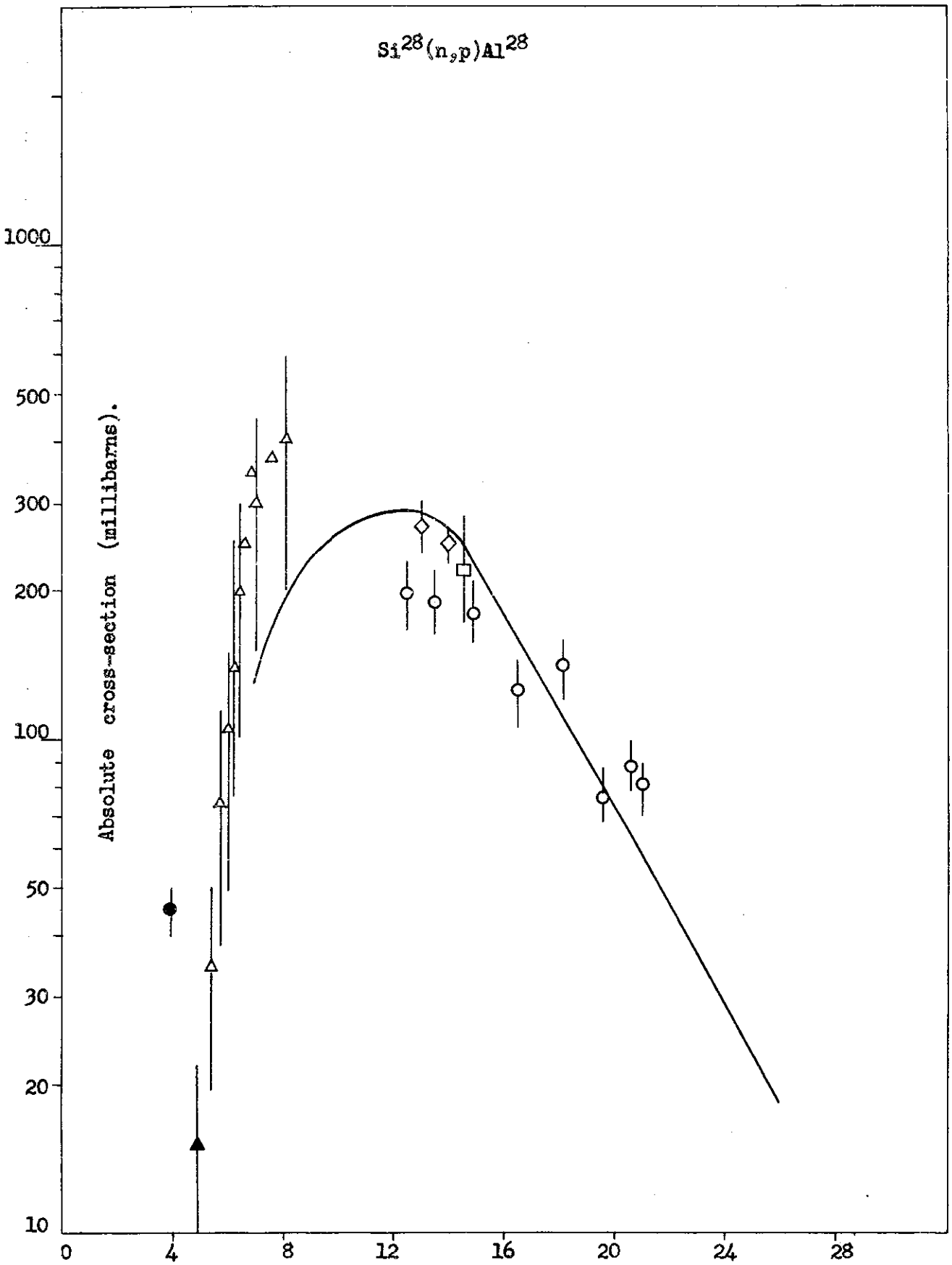
$Si^{28}(n,p)Al^{28}$
Absolute cross-section (millibarns).
1000
500
300
200
100
50
30
20
10
0
4
8
12
16
20
24
28
NEUTRON ENERGY (MEV).

FIG. 7

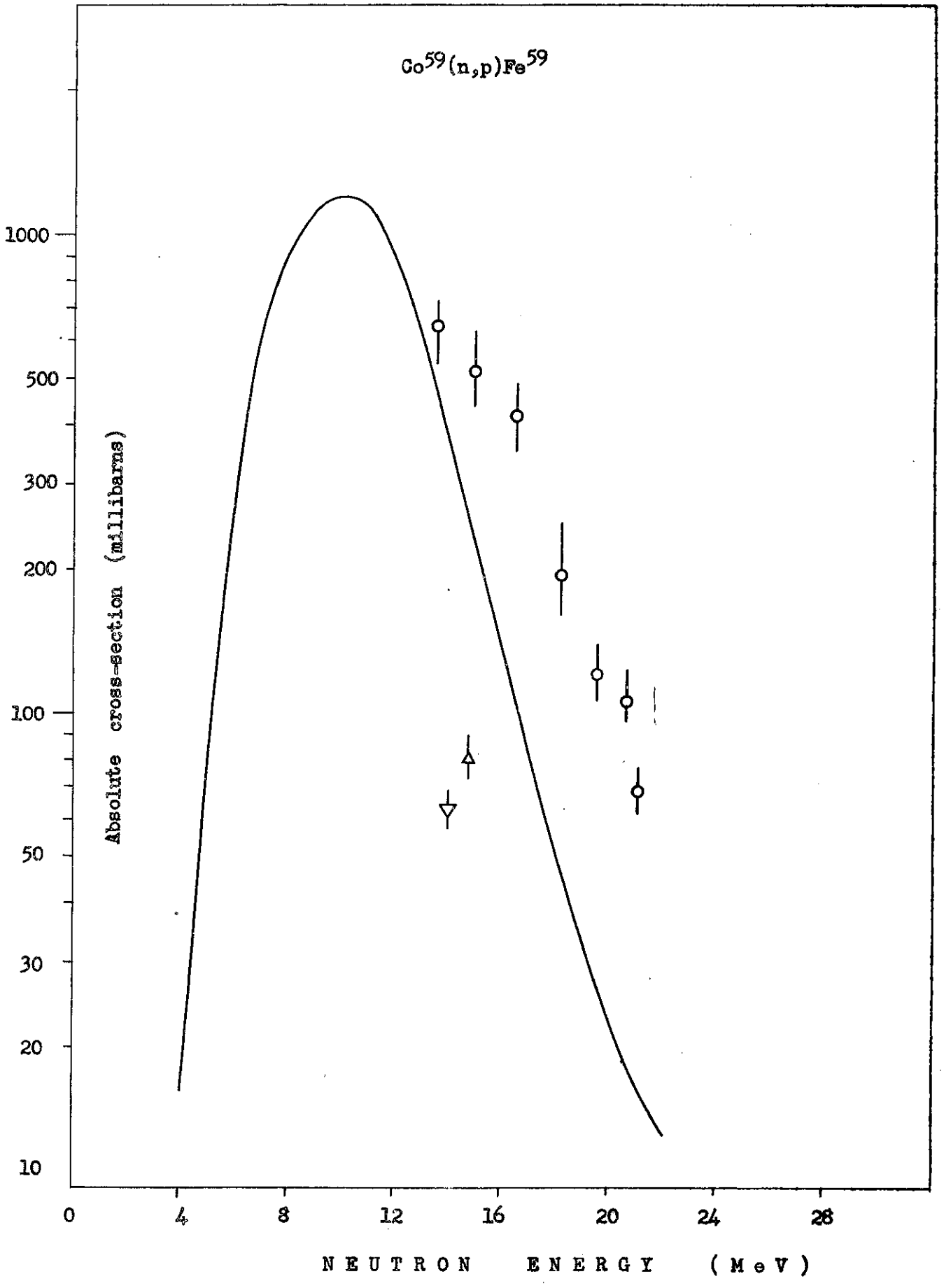
$Co^{59}(n,p)Fe^{59}$
Absolute cross-section (millibarns)
1000
500
300
200
100
50
30
20
10
0
4
8
12
16
20
24
28
NEUTRON ENERGY (MeV)

FIG. 8

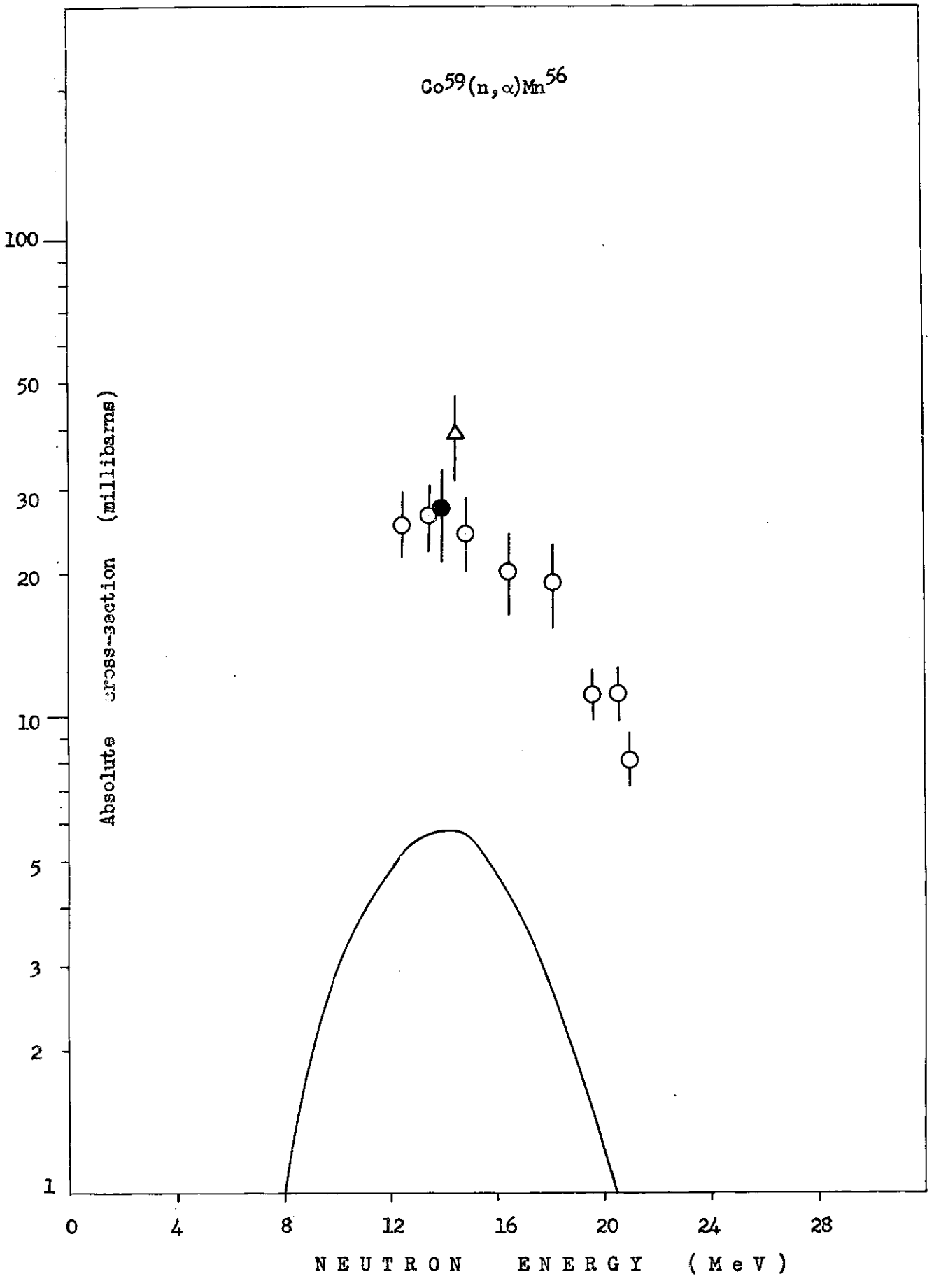
$Co^{59}(n,\alpha)Mn^{56}$
Absolute cross-section (millibarms)
100
50
30
20
10
5
3
2
1
0
4
8
12
16
20
24
28
NEUTRON ENERGY (MeV)

FIG. 9

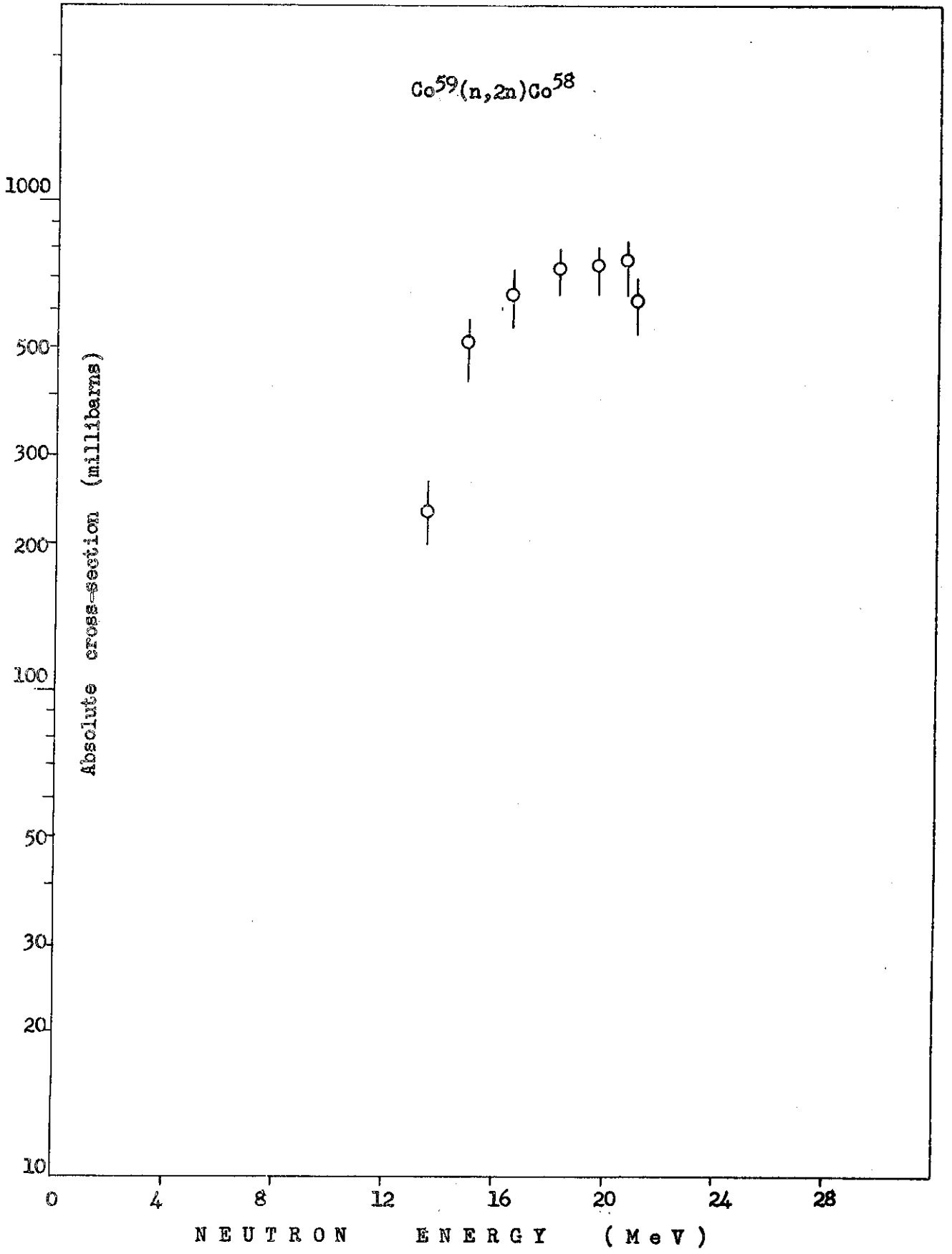
$Co^{59}(n,2n)Co^{58}$
Absolute cross-section (millibarns)
1000
500
300
200
100
50
30
20
10
0
4
8
12
16
20
24
28
NEUTRON ENERGY (MeV)

FIG. 10

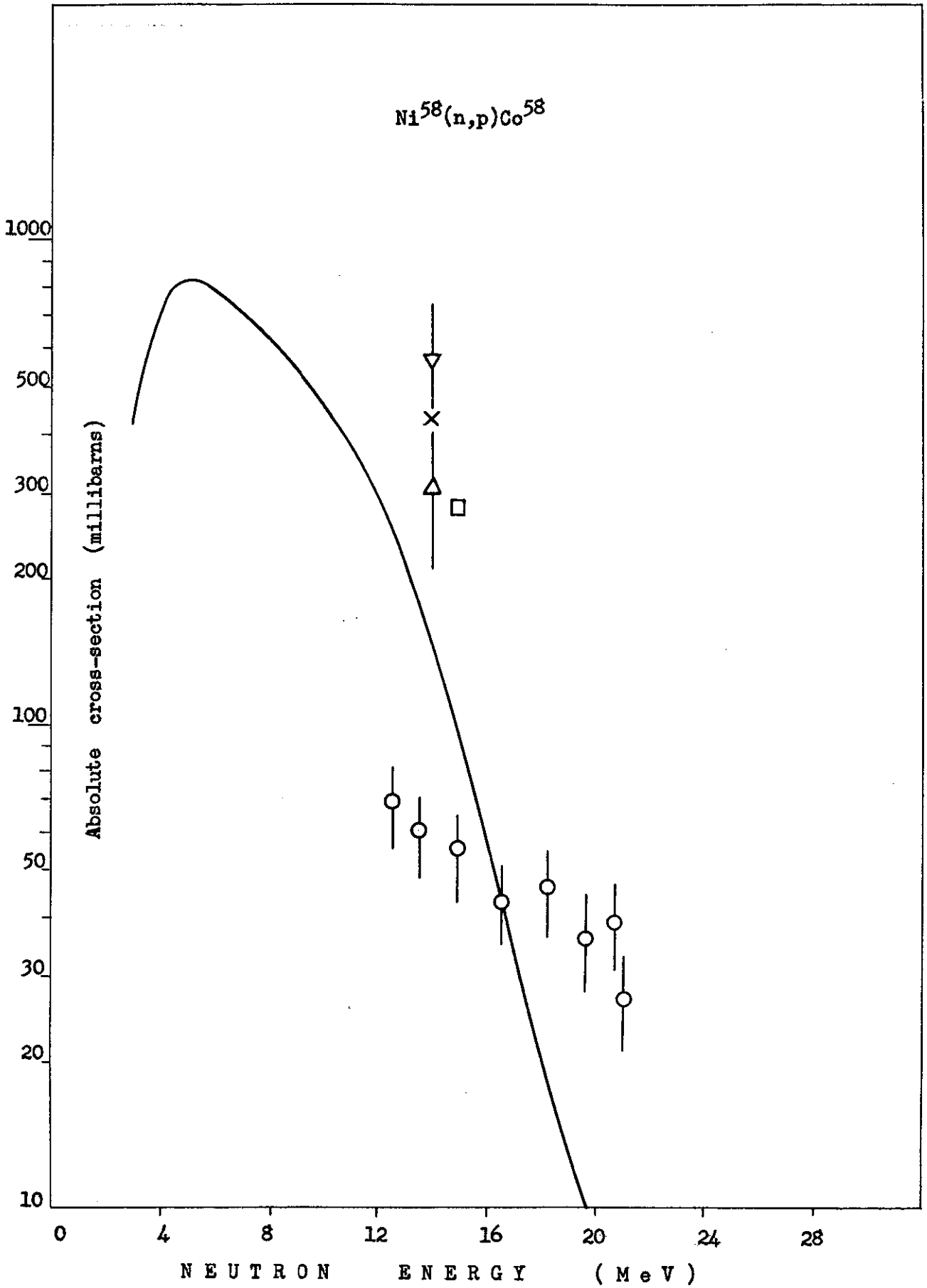
Ni58(n,p)Co58
Absolute cross-section (millibarns)
1000
500
300
200
100
50
30
20
10
0
4
8
12
16
20
24
28
NEUTRON ENERGY (MeV)

FIG. 11

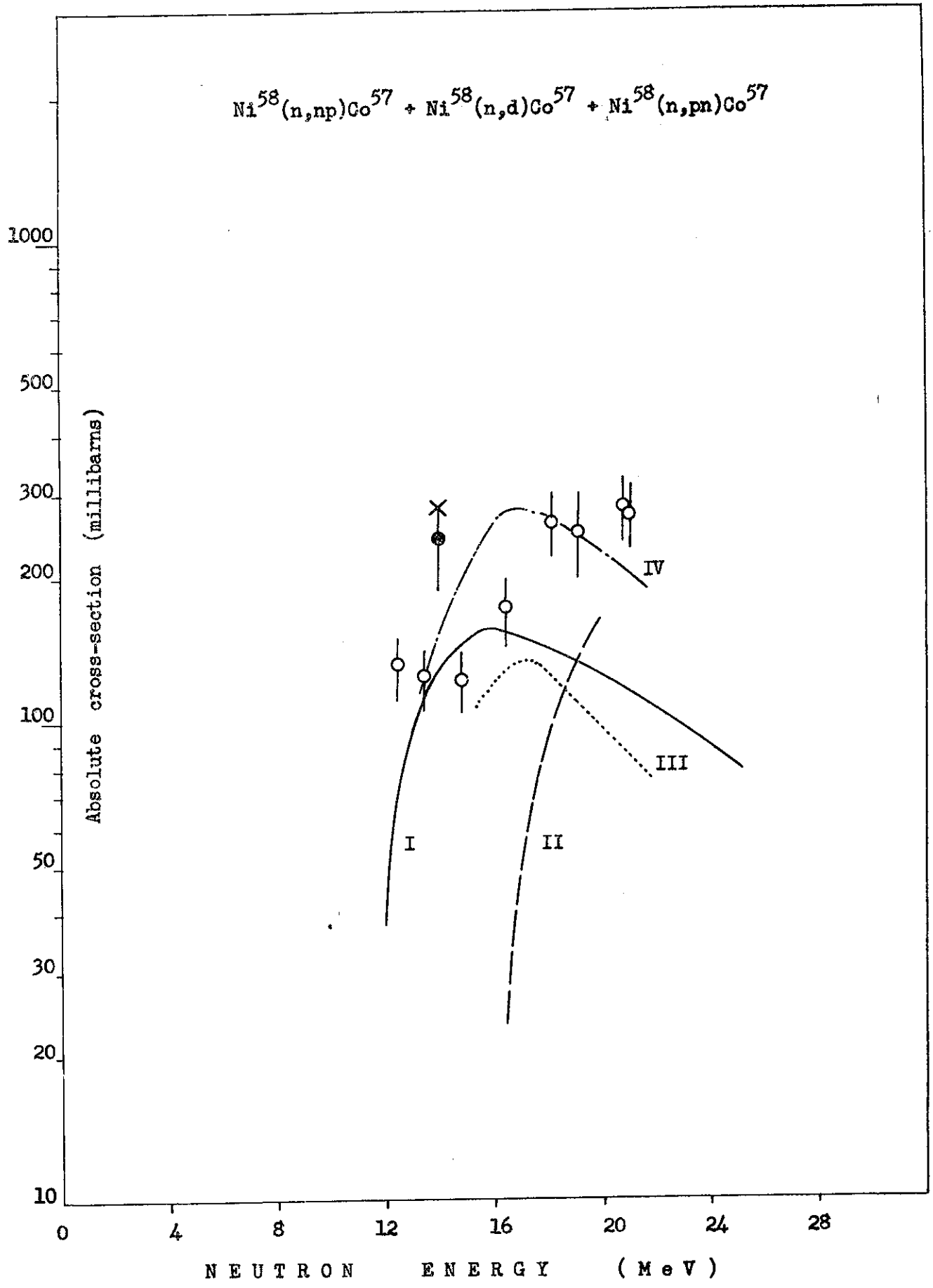
$Ni^{58}(n,np)Co^{57} + Ni^{58}(n,d)Co^{57} + Ni^{58}(n,pn)Co^{57}$
Absolute cross-section (millibarms)
1000
500
300
200
100
50
30
20
10
0
4
8
12
16
20
24
28
NEUTRON ENERGY (MeV)
I
II
III
IV

FIG. 12

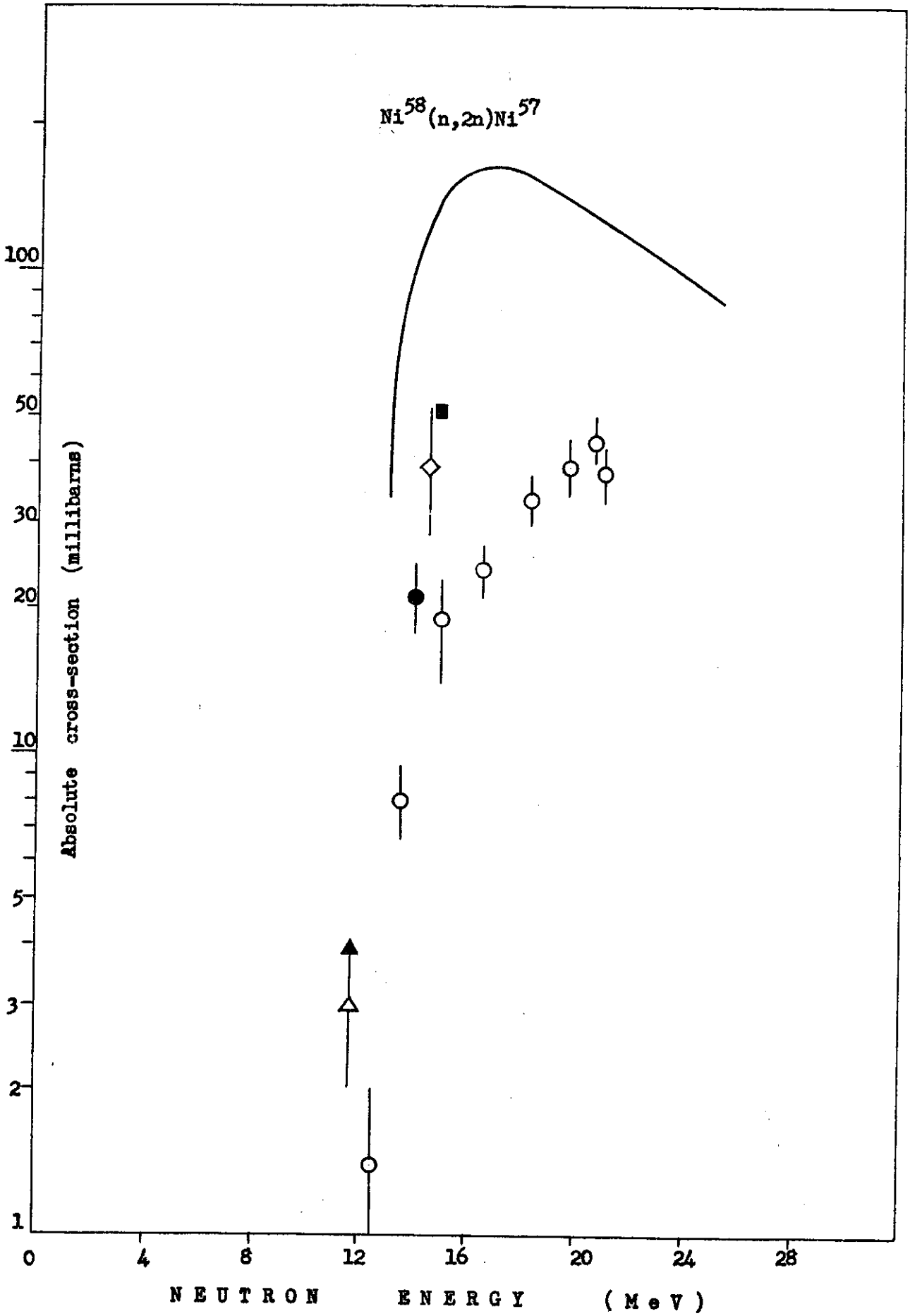
$Ni^{58}(n,2n)Ni^{57}$
Absolute cross-section (millibarns)
100
50
30
20
10
5
3
2
1
0
4
8
12
16
20
24
28
NEUTRON ENERGY (MeV)

FIG. 13

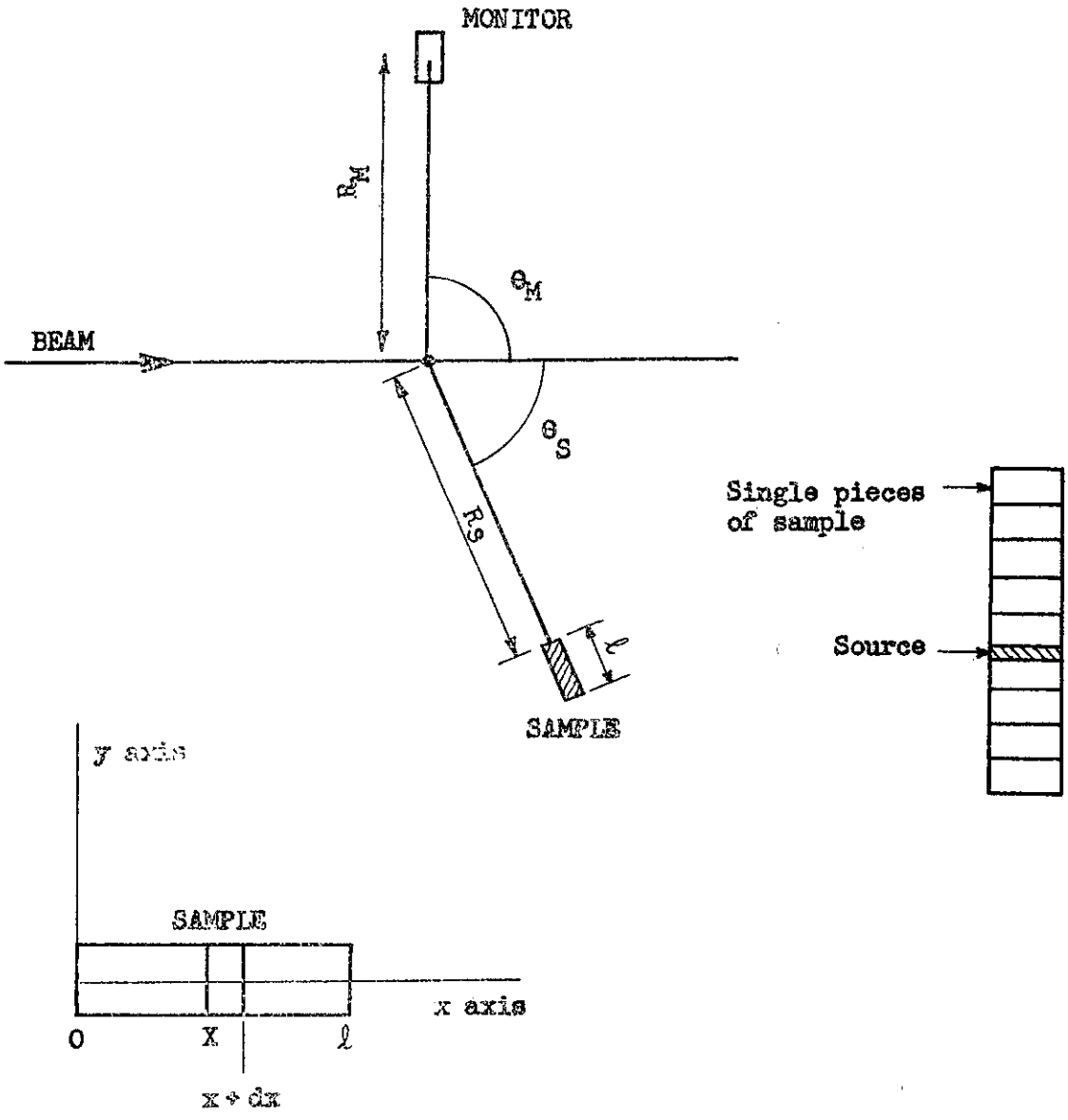
MONITOR
R_M
θ_M
BEAM
θ_S
R_S
ℓ
SAMPLE
Single pieces of sample
Source
y axis
SAMPLE
x axis
0
X
ℓ
x + dx

FIG. 14

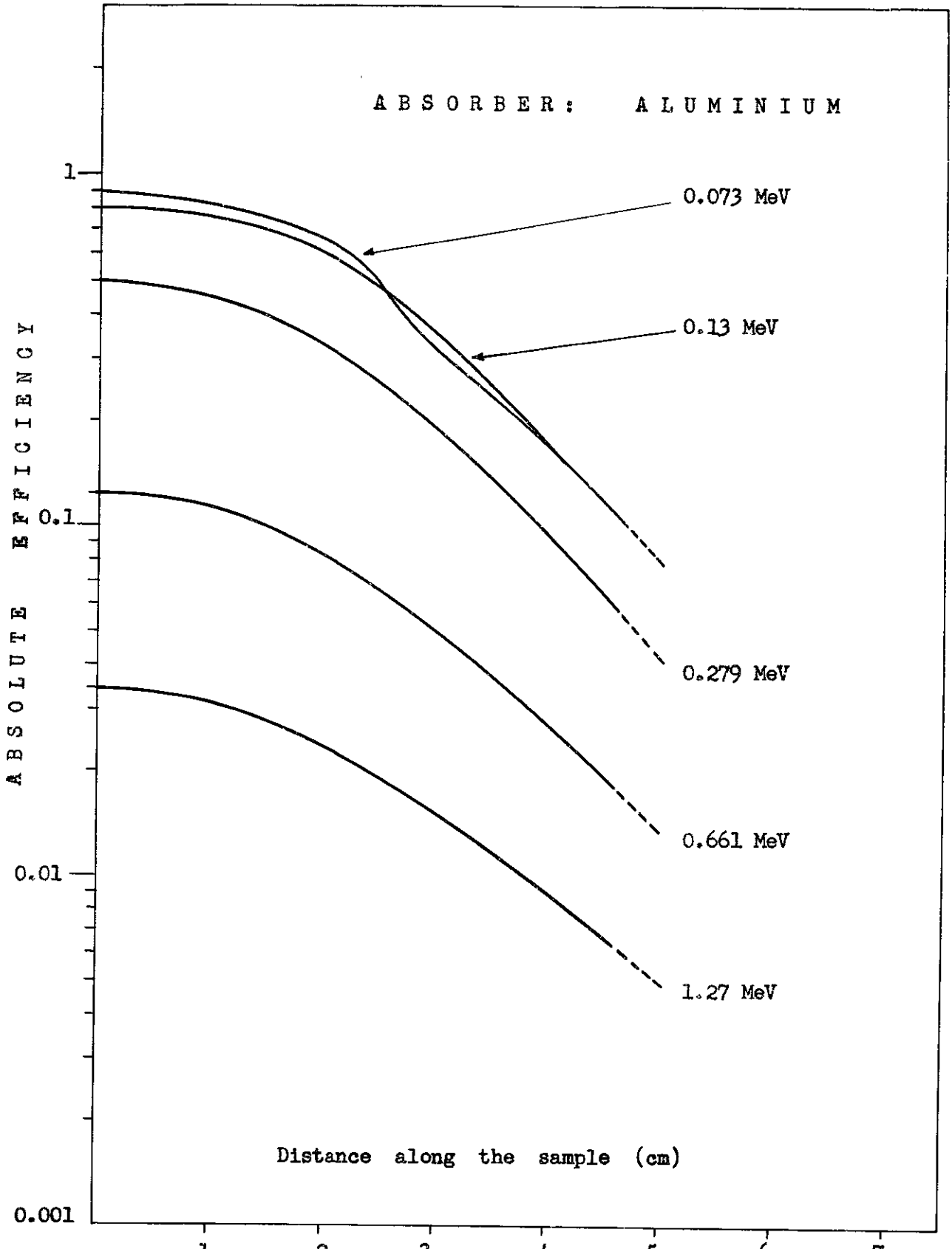
ABSORBER: ALUMINIUM
ABSOLUTE EFFICIENCY
1
0.1
0.01
0.001
0.073 MeV
0.13 MeV
0.279 MeV
0.661 MeV
1.27 MeV
Distance along the sample (cm)
1
2
3
4
5
6
7

FIG. 15

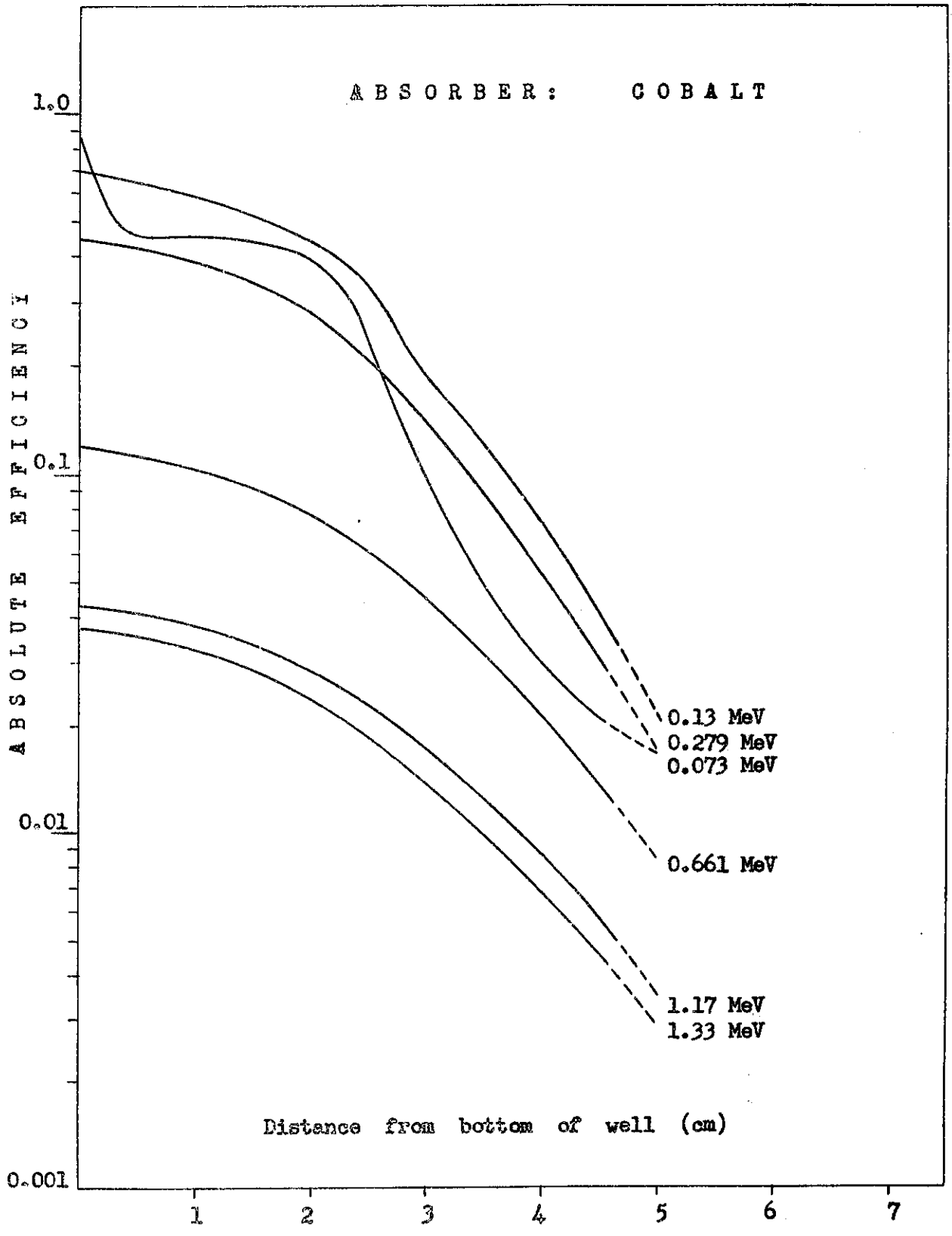
ABSORBER: COBALT
1.0
0.1
0.01
0.001
ABSOLUTE EFFICIENCY
0.13 MeV
0.279 MeV
0.073 MeV
0.661 MeV
1.17 MeV
1.33 MeV
Distance from bottom of well (cm)
1
2
3
4
5
6
7

FIG. 16

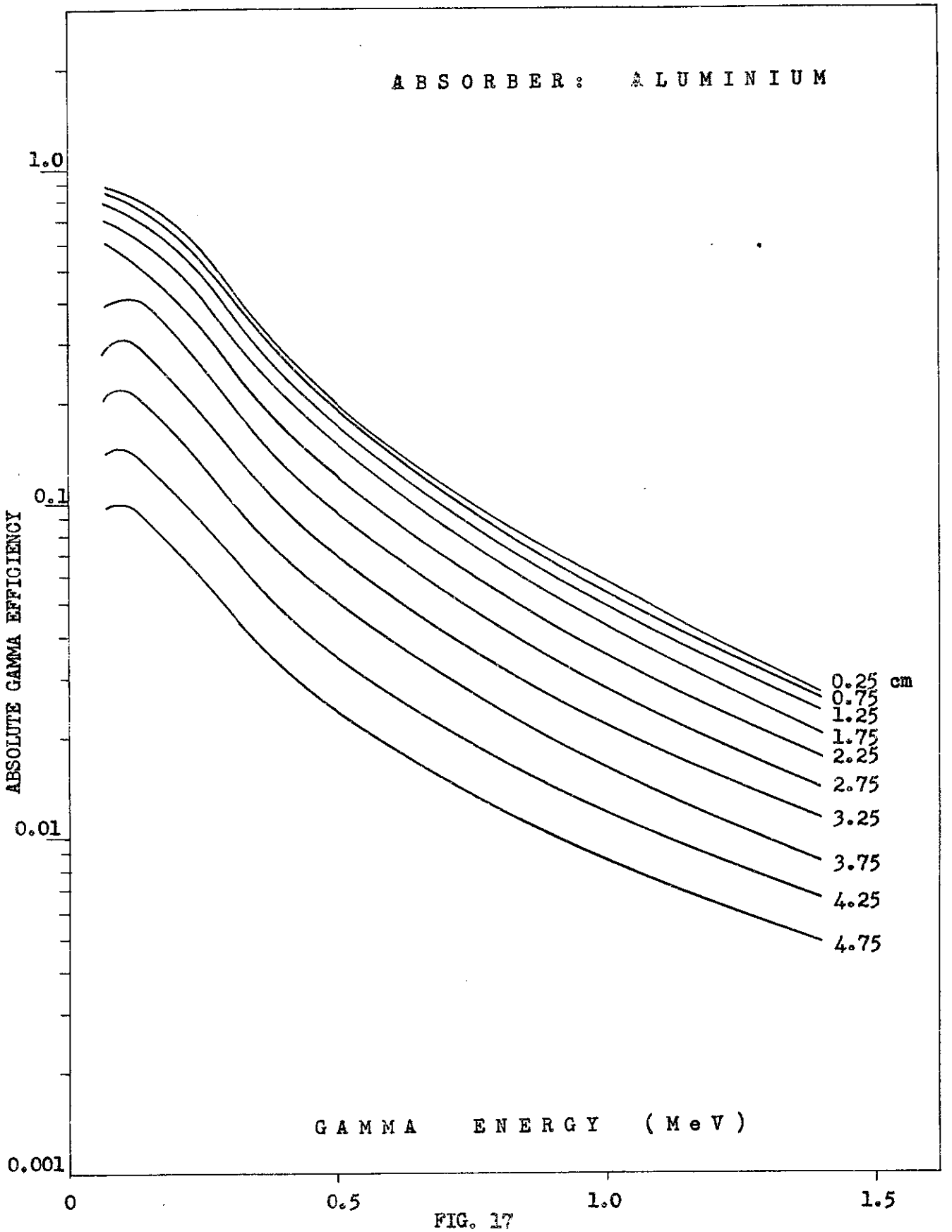
ABSORBER: ALUMINIUM
1.0
0.1
0.01
0.001
ABSOLUTE GAMMA EFFICIENCY
0.25 cm
0.75
1.25
1.75
2.25
2.75
3.25
3.75
4.25
4.75
GAMMA ENERGY (MeV)
0
0.5
1.0
1.5

FIG. 17

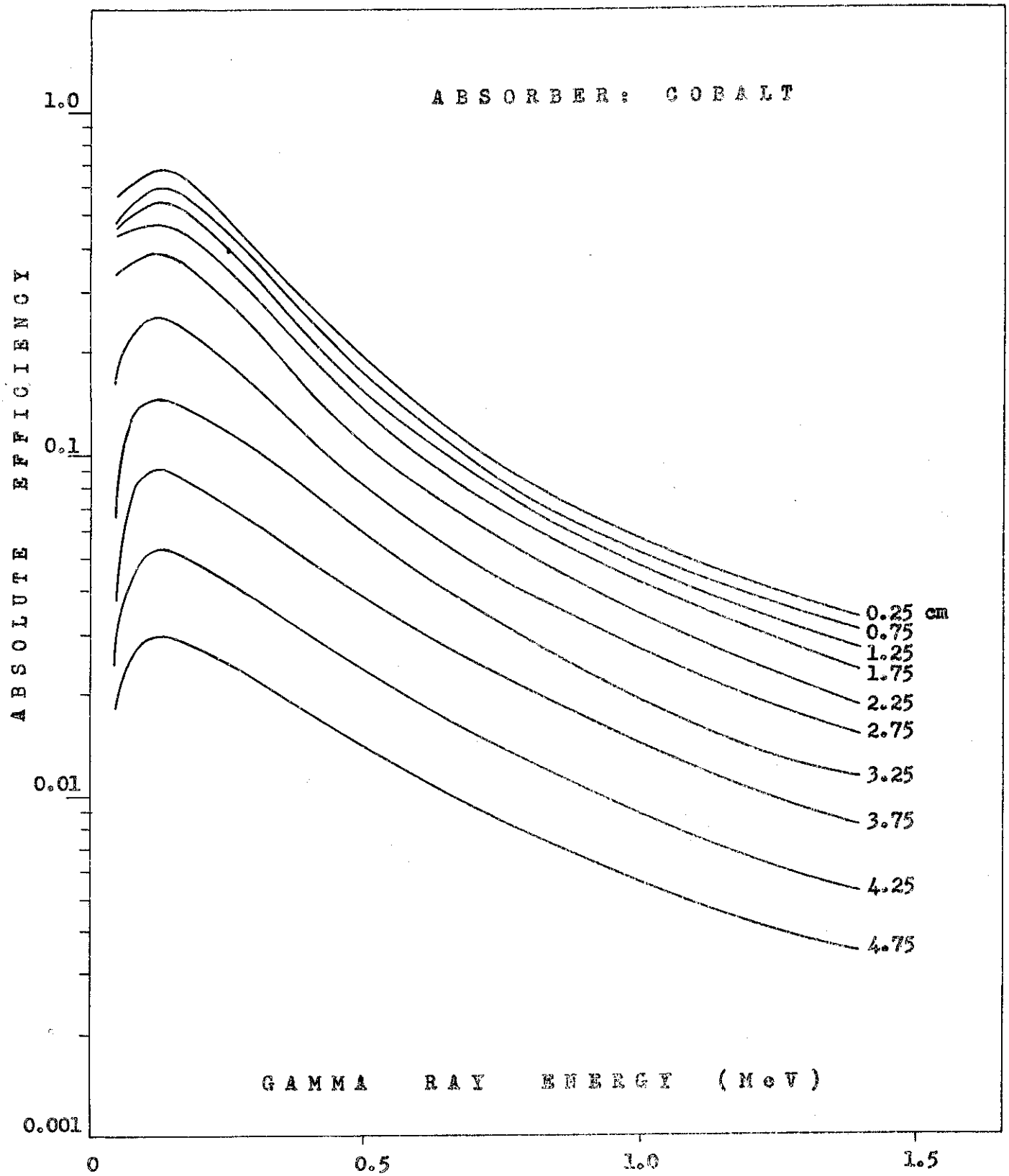
ABSORBER: COBALT
ABSOLUTE EFFICIENCY
1.0
0.1
0.01
0.001
0.25 cm
0.75
1.25
1.75
2.25
2.75
3.25
3.75
4.25
4.75
GAMMA RAY ENERGY (MeV)
0
0.5
1.0
1.5

FIG. 18